Journal of Translational Medicine

RESEARCH

Open Access

Deletion of MAPL ameliorates septic cardiomyopathy by mitigating mitochondrial dysfunction

Yinghua Wang[1†], Xiying Huang[1†], Huanhuan Huo[1], Zhaohua Cai[1], Qingqi Ji[1], Yi Jiang[2], Fei Zhuang[1], Yi Li[1], Linghong Shen[1], Xia Wang[1*] and Ben He[1*]

Abstract

Aim Mitochondrial dysfunction is a critical factor in the pathogenesis of septic cardiomyopathy (SCM). Mitochondrial anchored protein ligase (MAPL), a small ubiquitin-like modifier (SUMO) E3 ligase, plays a significant role in mitochondrial function. However, the role of MAPL in SCM remains unclear.

Methods To investigate the role of MAPL in SCM, cardiomyocyte-specific MAPL knockout mice were generated. A cecal ligation and puncture (CLP) procedure was employed to induce a sepsis-like condition.

Results The expression of MAPL in heart tissues and H9C2 cardiomyocytes was elevated following CLP challenge or lipopolysaccharide (LPS) stimulation. MAPL deficiency ameliorated CLP-induced cardiac injury, dysfunction, and inflammation, and also improved the survival rate of mice following CLP operation. Additionally, MAPL deficiency or knockdown inhibited LPS-induced cardiomyocyte apoptosis, improved mitochondrial structural abnormalities, and increased ATP production. Furthermore, MAPL knockdown mitigated LPS-induced reductions in mitochondrial membrane potential (MMP) and intracellular reactive oxygen species (ROS) production. Mechanistically, the expression of dynamin-related protein 1 (drp1) in the mitochondria of heart tissues or H9C2 cardiomyocytes was elevated under septic conditions. Accordingly, the SUMOylation of drp1 in heart tissues or H9C2 cardiomyocytes was increased under sepsis conditions, which was reduced by MAPL knockout or knockdown.

Conclusion Our results reveal that MAPL promotes cardiac injury/dysfunction and inflammation in SCM. Deficiency or knockdown of MAPL alleviates SCM by reducing drp1 SUMOylation as well as drp1-mediated mitochondrial dysfunction. These findings suggest that targeting MAPL may represent a therapeutic strategy for patients with SCM.

Keywords MAPL, Mitochondria, SUMOylation, Septic cardiomyopathy

†Yinghua Wang and Xiying Huang contributed equally to this work.

*Correspondence:
Xia Wang
wangxia31610@163.com
Ben He
heben241@126.com
[1]Department of Cardiology, Shanghai Chest Hospital, Shanghai Jiao Tong University School of Medicine, Shanghai, China
[2]Department of Cardiovascular Surgery, Shanghai Chest Hospital, Shanghai Jiao Tong University School of Medicine, Shanghai, China

Introduction

Sepsis, a life-threatening condition characterized by multi-organ dysfunction, is often precipitated by autoimmune responses secondary to infection. It is the leading cause of mortality in intensive care units. SCM, an acute cardiac injury marked by compromised left ventricular systolic and diastolic function, frequently manifests as a complication of sepsis [1–3]. Our prior research indicated that SCM has a mortality rate exceeding 50%, with brain natriuretic peptide (BNP) identified as the most reliable clinical marker for predicting SCM post-thoracic surgery [3]. To date, no specific therapeutic strategies for SCM are available.

A thoroughly investigated pathological feature is mitochondrial dysfunction, which is likely to contribute to cardiac dysfunction through the depletion of myocardial energy. Consequently, ameliorating mitochondrial dysfunction may represent a valuable therapeutic strategy for preventing sepsis-related multiple organ dysfunction syndrome [4]. However, the underlying molecular mechanisms of mitochondrial dysfunction during SCM remain unclear.

MAPL (MULAN, GIDE, or MUL1), a ubiquitin or SUMO E3 ligase anchored to the outer membrane of mitochondria, has been identified in previous studies as a potential therapeutic target for diseases associated with mitochondrial dysfunction [5]. Inhibition of MAPL mitigates phenylephrine-induced cardiac hypertrophy by modulating mitochondrial dynamics [6]. Several factors associated with mitochondrial dynamics, including mitochondrial fusion and fission, have been identified as target genes of MAPL. MAPL has been shown to facilitate mitochondrial fission by mediating the SUMOylation of drp1, a GTPase critical for this process [7]. The increase in drp1 SUMOylation results in elevated drp1 protein levels and a more stable association with the mitochondrial membrane [8]. Furthermore, MAPL functions as a ubiquitin E3 ligase that targets mitochondrial fusion protein-2 (mfn2) for ubiquitination and subsequent degradation, thereby preventing mitochondrial hyperfusion [9, 10]. Given the role of MAPL in regulating mitochondrial dynamics, we aimed to study whether it would affect mitochondrial function during SCM.

In the present study, we observed a significant upregulation of MAPL expression in cardiomyocytes following CLP challenge or LPS stimulation. Notably, MAPL deficiency markedly mitigated sepsis-induced cardiac dysfunction, inflammation, and apoptosis. Mechanistically, MAPL facilitates mitochondrial fission by SUMOylating drp1, leading to drp1 accumulation in cardiomyocytes. These findings indicate that targeting MAPL may represent a novel therapeutic strategy for treating SCM.

Materials and methods

Animals

Male C57BL/6 mice (age: 8–12 weeks; weight 20–30 g) were purchased from Shanghai JieSiJie Experimental Animal Co., Ltd (Shanghai, China). $MAPL^{flox/flox-Myh6-iCre}$ were established by GemPharmatech Co., Ltd (Nanjing, Jiangsu Province, China). MAPL cardiomyocyte-specific knockout (MAPL CKO) mice were generated using CRISPR/Cas9 technology. According to the structure of MAPL gene, exon2-exon4 of the MAPL-201 (ENSMUST00000044058.10) transcript was recommended as the knockout region. Cas9, sgRNA and Donor were microinjected into fertilized eggs of C57BL/6JGpt mice. Fertilized eggs were transplanted to pseudo-pregnant female mice. After crossing among heterogeneous mice, a stable homozygous mutant line was identified with DNA sequencing. The $MAPL^{flox/flox}$ mice were mated with mice expressing Myh6-iCre recombinase, resulting in the loss of function of MAPL in cardiomyocytes.

All the animals were acclimatized in a room (12/12 hour light/dark cycle; 25±2℃) and allowed free access to diet and water. The Medical Ethics Committee of Shanghai Jiao Tong University approved all animal experiments (KS(Y)23070), which were conducted in accordance with the National Institutes of Health Guide for the Care and Use of Laboratory Animals.

Mouse model

The septic mouse model was established by CLP as previously described [11]. Briefly, CLP procedures were as follows: mice were anesthetized with isoflurane. The abdominal skin was sterilized with iodine, and a 1 cm laparotomy was performed on the left side of the mediventral line under the xiphoid to expose the cecum. The distal end of the cecum was ligated by a 4−0 silk suture and punctured through to through with a 21-gauge needle. Then feces (0.2 ml) were extruded. The peritoneum, fasciae and abdominal musculature was closed by running sutures. 1 ml pre-warmed sterile 0.9% saline was percutaneously injected after the establishment of CLP. Mice were divided into four groups: WT-sham ($MAPL^{flox/flox}$ wild-type mice), WT-CLP, CKO ($MAPL^{flox/flox-Myh6-iCre}$)-sham and CKO-CLP.

LPS-induced SCM was performed by intraperitoneal injection of LPS at different doses (E.coli, 0111:B4, Sigma, Germany, L2630). After 12 h of LPS injection, cardiac function was assessed using M-mode echocardiography, and then all mice were sacrificed.

Human subjects

Myocardium samples used in this study were obtained from patients with infective endocarditis or degenerative valve regurgitation who underwent valve replacement or repair surgery. All procedures involving human

specimens in this study was approved by The Ethics Committee Board of Shanghai Chest Hospital, Shanghai Jiao Tong University School of Medicine (IS23057). All procedures complied with ethical guidelines of the Declaration of Helsinki.

Echocardiogram evaluation

Echocardiographic analysis was performed using a Vevo 2100 High-Resolution Digital-Imaging System (Visual Sonics, Toronto, Canada) equipped with an MS400 transducer. Briefly, mice were anesthetized using isoflurane (1.5% mixed with oxygen), andthen gently kept on heating pads (37℃). Ventricular M mode ultrasound was performed at the papillary muscle level to assess left ventricular function, left ventricular diastolic and systolic diameter.

Establishment of MAPL knockdown H9C2 cardiomyocyte lines and cell culture

Plasmid of shMAPL (NM_001106695.1), shNC, paPAX2 and second-generation lentiviral packaging plasmid (Addgene Catalog 12260) were transfected by lipo3000 into HEK293T cells. H9C2 cardiomyocytes obtained from National Collection of Authenticated Cell Cultures (Chinese Academy of Sciences, China) were cultured in high glucose Dulbecco's modified Eagle's medium (purchased from Thermo, USA) supplemented with 10% fetal bovine serum (Gibco, USA) and 1% penicillin/streptomycin (Thermo, USA) at 37℃ in a humidified incubator of 5% CO_2 and 95% air. Then, H9C2 cardiomyocytes were infected with shMAPL or shNC lentiviruses for 8 h and screened by 5ug/ml puromycin for 1 week. The sequence of shMAPL is as follows:

Forward:

CCGGCGCCGTACTGTACTCCATATACTCGAGAAATAGTCATTCCACAGGTGGGTTTTG;

Reverse:

AATTCAAAACCCACCTGTGGAATGACTATTCTCGAGTATATGGAGTACAGTACGGCGCCGG.

Cell treatment

H9C2 cardiomyocytes were cultured in high glucose Dulbecco's modified Eagle's medium with 10% fetal bovine serum and 1% penicillin/streptomycin at 37℃ under 5% CO_2. When the cells reached 70% confluency, LPS (20 μg/ml) was added to the cell culture and incubated for 24 h to establish the LPS-induced cell injury model.

Transfection assay

H9C2 cardiomyocytes were seeded and transfected with MAPL-overexpression (MAPL-OE) plasmid (HanBio, Shanghai, China) using Lipofectamine™ 3000 (Thermo Fisher Scientific, L3000075, USA) following the manufacturer's instructions.

Mitochondria isolation and purification

Mitochondria were isolated and purified by Qproteome Mitochondria Isolation Kit (QIAGEN, Germany, 37612). Mitochondrial Lysis Buffer were used to lysate cells or homogenate tissue. After centrifugation at 1000 g for 10 min at 4 °C, the pellet was resuspended in the Mitochondrial Disruption Buffer. The lysate was drawn into a blunt-ended needle syringe and ejected with one stroke to disrupt cells completely. Then the lysate was recentrifuged at 1000 g for 10 min at 4 °C. Finally, the supernatant was re-centrifuged at 6000 g for 10 min at 4 °C and the pellet was mitochondria. Mitochondria were collected, washed and resuspended in the Mitochondrial Storage Buffer.

Western blotting analysis

Total protein was extracted from heart tissues and purified mitochondria and cells using the RIPA lysis buffer with phosphatase inhibitor (Roche, Switzerland). The protein concentration was determined using a BCA protein concentration assay kit. Equal amounts (30–50 μg) of proteins were subjected to 12% SDS-PAGE and transferred to a PVDF membrane. The membrane was blocked with 5% fat-free milk at room temperature for 1 h and incubated with the following primary antibodies: MAPL (1:1000, abcam, USA), SUMO1 (1:1000, Cell Signaling Technology, USA), drp1 (1:1000, Cell Signaling Technology, USA), mfn2 (1:1000, Cell Signaling Technology, USA), SUMO2/3 (1:1000, Cell Signaling Technology, USA), COX-IV (1:1000, Cell Signaling Technology, USA), VDAC1 (1:1000, Cell Signaling Technology, USA), Caspase3 (1:1000, Cell Signaling Technology, USA), Caspase 8 (1:1000, Cell Signaling Technology, USA), RIPK3 (1:1000, Cell Signaling Technology, USA), β-actin (1:1000, Cell Signaling Technology, USA), Bcl2 (1:1000, Cell Signaling Technology, USA), Bax (1:1000, Cell Signaling Technology, USA), α-tubulin (1:1000, Beyotime, China) at 4℃ overnight. On the second day, after 1 h of incubation with HRP-conjugated secondary antibodies, the membrane was detected by enhanced chemiluminescence(ECL). Image analysis was performed using the Amersham Image680 Scanning machine, and intensity was quantified using the Image J software. The optical density was normalized to that of COX-IV, VDAC1, β-actin or α-tubulin representing relative optical density.

Immunofluorescence staining

H9C2 cardiomyocyte lines were seeded on circular coverslips. Cells were fixed with 4% formaldehyde for 10 min, followed by permeabilization with 0.1% Triton X-100 in PBS for 5 min. Cells were blocked with 2% BSA at room temperature for 60 min and then incubated with the primary antibodies of anti-MAPL (1:100, abcam),

anti-TOMM20 (1:100, Beyotime), anti-Bax (1:100, Beyotime) at 4℃ overnight. Following incubation, the samples were washed with PBS and incubated with the secondary antibody (Beyotime, A0516, A0568). The nuclei were stained with DAPI. The coverslips were mounted using 90% glycerol in PBS, and fluorescence was detected with light and fluorescence microscopy.

Transmission electron microscopy (TEM)

After euthanasia, mice were immediately transcardially perfused with 0.1 M PBS (PH 7.4). Heart tissues were collected, dissected into 1-2mm^3 pieces, and fixed in 2.5% glutaraldehyde and 0.1 M sodium cacodylate buffer at 4℃. Cells were collected in centrifuge tubes and fixed with 2.5% glutaraldehyde and 0.1 M sodium cacodylate buffer at 4℃. The collected samples were embedded, subjected to ultramicrotomy to obtain 90 nm thin sections, and captured using a Hitachi H-7650 transmission electron microscope (Hitachi, Japan).

Enzyme-linked immunosorbent assay (ELISA)

The serum was obtained from blood after centrifugation at 3000 rpm for 15 min. Mice serum cytokine was detected using the ELISA assay kits: cTnI and BNP (Elabscience, Texas, USA, E-EL-M1203, E-EL-M0204); CRP (Beyotime, Shanghai, China, PC186), IL-1α (Beyotime, Shanghai, China, PI561), IL-1β (Beyotime, Shanghai, China, PI301), IL-6 (Beyotime, Shanghai, China, PI326), TNFα (Beyotime, Shanghai, China, PT513); LPS (Camilo Nanjing, China, 2P-KMLJ942143p) according to the manufacturer's instructions.

RNA isolation and real-time quantitative PCR (RT-qPCR) analysis

Total RNA was extracted from tissues and cells using TRIzol reagent, and 1 μg of total RNA was reverse transcribed into cDNA using a TAKARA PrimeScript™ RT reagent kit with gDNA eraser (TAKARA, Japan, RR047A). cDNA (1μL) was then mixed with qPCR SYBR® Premix Ex Taq™ (Perfect Real Time) Kit and 50μM primers to obtain a final volume of 10μL, which was subjected to quantitative real-time PCR using an S1000 thermal cycler Realtime PCR System (Applied Biosystems, CA, USA). The primers used to determine the expression of specific genes are listed as followed. The relative mRNA expression of specific genes was quantified using the comparative ΔΔCT method and normalized to β-actin or GAPDH.

The primers of MAPL were as followed:

MAPL-mouse-F	GAGCTGTGCGGTCTGTTAAAG
MAPL-mouse-R	GGTAGTTCGGTTCCACACCA
MAPL-rat-F	ACGAGGACGGTGTGGCTATGG
MAPL-rat-R	GATGGCATCGGTGAAGGACTGTAC

Co-immunoprecipitation (co-IP) assays

Equal weights of heart tissues from mice or cells were lysed with RIPA lysis buffer containing a protease inhibitor. Total cell extracts were centrifuged at 12,500 rpm for 25 min at 4 °C. The purified proteins were resolved in Pierce™ IP Lysis Buffer (Thermo Fisher Scientific, 87788). Magnetic bands Pierce™ Protein A/G Magnetic Beads (Thermo Fisher Scientific, 88802) and anti-drp1 (1:100, Cell Signaling Technology, USA)antibody were added to the cell lysates and incubated at 4 °C overnight. Then the bead-antibody-antigen complexes were collected using a magnetic separator and washed five times with IP lysis buffer. The lysate were eluted and denatured by boiling with 30μL 2xSDS loading buffer at 100℃ for 5 min, followed by SDS-PAGE or mass spectrometry analysis. The IgG antibody was used as a negative control.

ROS detection

DCFH-DA staining was performed to monitor ROS levels according to the instructions. In brief, cells were treated with 5mM DCFH-DA solution (Beyotime, S0033S) at 37 °C for 20 min. Then, cells were washed three times with warm serum-free DMEM, and the level of ROS was examined with a fluorescence microscope. In addition, N-acetyl-L-cysteine (NAC) (Beyotime, Shanghai, China, S0077) was preincubated at a concentration of 5 mM for 1 h before ROS detection. The following steps were conducted as mentioned above.

TUNEL staining

Following manufacturer instructions TUNEL staining was performed using the TUNEL BrightGreen Apoptosis Detection Kit (Vazyme Biotech Co., Ltd., Nanjing, China). The prepared samples were washed three times with PBS and fixed with 4% paraformaldehyde for 10 min. After incubation with 0.2% Triton X-100 for 5 min, 50 μl of TUNEL assay solution was added to the samples and stained at 37℃ away from the light for 60 min. Apoptotic nuclei were labeled with green fluorescein staining and total cardiomyocyte nuclei were marked with DAPI. The pictures of heart tissues were viewed by confocal microscopy (LSM700, Zeiss, Jena, Germany).

Measurement of Oxygen Consumption Rate (OCR)

Oxygen consumption rate (OCR) was measured with an Agilent Seahorse XFe24 Extracellular Flux Analyzer (Seahorse Bioscience, USA). Cells were seeded in an XF 24-well cell culture microplate at 40,000 cells per well (Seahorse Bioscience, USA) in 250 μl of DMEM and incubated for 24 h at 37 °C under a 5% CO_2 atmosphere. The growth medium was replaced with 575 μl of pre-warmed bicarbonate free DMEM, pH 7.4, and cells

were incubated at 37 °C for 1 h before starting the assay. After baseline measurements, OCR was measured after sequentially adding to each well 75 µl of oligomycin, 75 µl of carbonyl cyanide-4-(trifluoromethoxy) phenylhydrazone (FCCP), 75 µl of rotenone and 75 µl of antimycin-A to reach working concentrations of (1 µM, 1 µM and 0.5 Mm respectively). OCR values were normalized to cell number at the time of seeding. Furthermore, time dependent studies were normalized to basal respiration following a standard protocol.

Statistical analysis

Data are presented as means ± SE and all statistical analysis was accomplished by GraphPad Prism 9.5.0 software. D'Agostino-Pearson omnibus normality test was performed to confirm that data are normally distributed followed by the Student's t-test (two-tailed, unpaired, and equal variance) for comparisons between two groups. For data comparison involving more than two groups, ANOVA is followed by Bonferroni's multiple comparison test. Survival was analyzed by the Kaplan-Meier method and log-rank test. Statistical values, including number of replicates (n), are noted in the figure legends.

Results

The expression of MAPL in H9C2 cardiomyocytes or heart tissues increases following LPS stimulation or CLP challenge

H9C2 cardiomyocytes were stimulated with LPS for various durations. The results demonstrated a significant elevation in MAPL protein levels at 1, 3, 6, 12, and 24 h post-LPS treatment (Fig. 1A). Consistently, immunofluorescence analysis indicated that MAPL expression was up-regulated in H9C2 cardiomyocytes after 24 h of LPS stimulation (Fig. 1B). To validate the expression of MAPL in vivo, CLP, a standard procedure to induce sepsis was performed in mice and then heart tissues post-CLP were collected at 3, 6, and 12 h for WB and RT-PCR analyses. Our results showed that the protein level of MAPL was up-regulated at 3, 6 and 12 h after CLP, while the mRNA level of MAPL was increased at 3 h and then decreased gradually (Fig. 1C and Fig. S1). Moreover, LPS-induced mice with sepsis were exhibited impaired cardiac function, as evidenced by a dose-dependent reduction in left ventricular ejection fraction (LVEF) (Fig. S2A). In addition, the protein level of MAPL increased in a dose-dependent manner following LPS stimulation (Fig. S2B). These results suggest that MAPL expression increases under septic condition.

MAPL deficiency improves myocardial function and attenuates inflammation in CLP-induced sepsis

To explore the role of MAPL in SCM, we generated the cardiomyocyte-specific MAPL-knockout mice ($MAPL^{CKO}$) by crossing the $MAPL^{flox/flox}$ mice with transgenic mice expressing Cre recombinase specifically in cardiomyocytes (Myh6-Cre mice). RT-PCR and WB analyses demonstrated MAPL deficiency at the mRNA and protein levels in the heart tissues of MAPL CKO mice (Fig. 2A, B and Fig. S3).

Subsequently, CLP was performed on the mice, and cardiac function was assessed via echocardiography at 3, 6, and 12 h post-CLP. The mice exhibited impaired cardiac function, as evidenced by a reduction in left ventricular ejection fraction (LVEF), cardiac output (CO) and left ventricular end-diastolic diameter (LVDd) from 6 h post-CLP (Fig. S4A-D). Therefore, in the subsequent study, echocardiography was conducted on age-matched wild-type (WT) and MAPL CKO mice 6 h after the CLP procedure. Our results demonstrated that MAPL deficiency mitigated the CLP-induced reduction in left ventricular ejection fraction (LVEF) and fractional shortening (FS: calculated by measuring the percentage change in left ventricular diameter during systole) (Fig. 2C-D), suggesting an improvement in myocardial dysfunction due to MAPL deficiency. Additionally, we monitored the survival rate of mice for 70 h post-CLP. The findings indicated that MAPL deficiency increased the survival rate of mice following CLP (Fig. 2E). Nonetheless, it is important to note that all mice in both groups died within 70 h post-CLP. We conducted an ELISA to quantify the serum levels of BNP and cTnI, biomarkers indicative of heart failure and cardiac injury, respectively. Consistent with expectations, WT mice exhibited elevated levels of both BNP and cTnI following CLP, which were inhibited by MAPL deficiency (Fig. 2F-G). Subsequently, we investigated whether MAPL knockout mitigates CLP-induced inflammation. As illustrated in Fig. 2H-J and Fig. S5, the CLP-induced increase in serum IL-1α, IL-1β, IL-6, TNFα and CRP levels was significantly attenuated in MAPL-CKO mice. However, the serum LPS levels remained unaltered, indicating that the production of LPS caused by CLP did not differ between the MAPL-WT and CKO groups (Fig. 2K). These findings suggest that cardiomyocyte-specific MAPL deficiency enhances cardiac function and mitigates inflammation in SCM.

MAPL deficiency mitigates cardiomyocyte apoptosis during SCM

Given our previous findings that MAPL deficiency attenuates CLP-induced inflammation, we investigated whether MAPL influences cardiomyocyte apoptosis. Western blot analysis demonstrated that MAPL knockdown or knockout inhibited the LPS- or CLP-induced upregulation of Bax and cleaved caspase-3, and prevented the downregulation of Bcl-2 (Fig. 3A-B). However, LPS-induced protein changes of Bcl-2 and Bax in H9C2 cardiomyocytes were not altered after MAPL

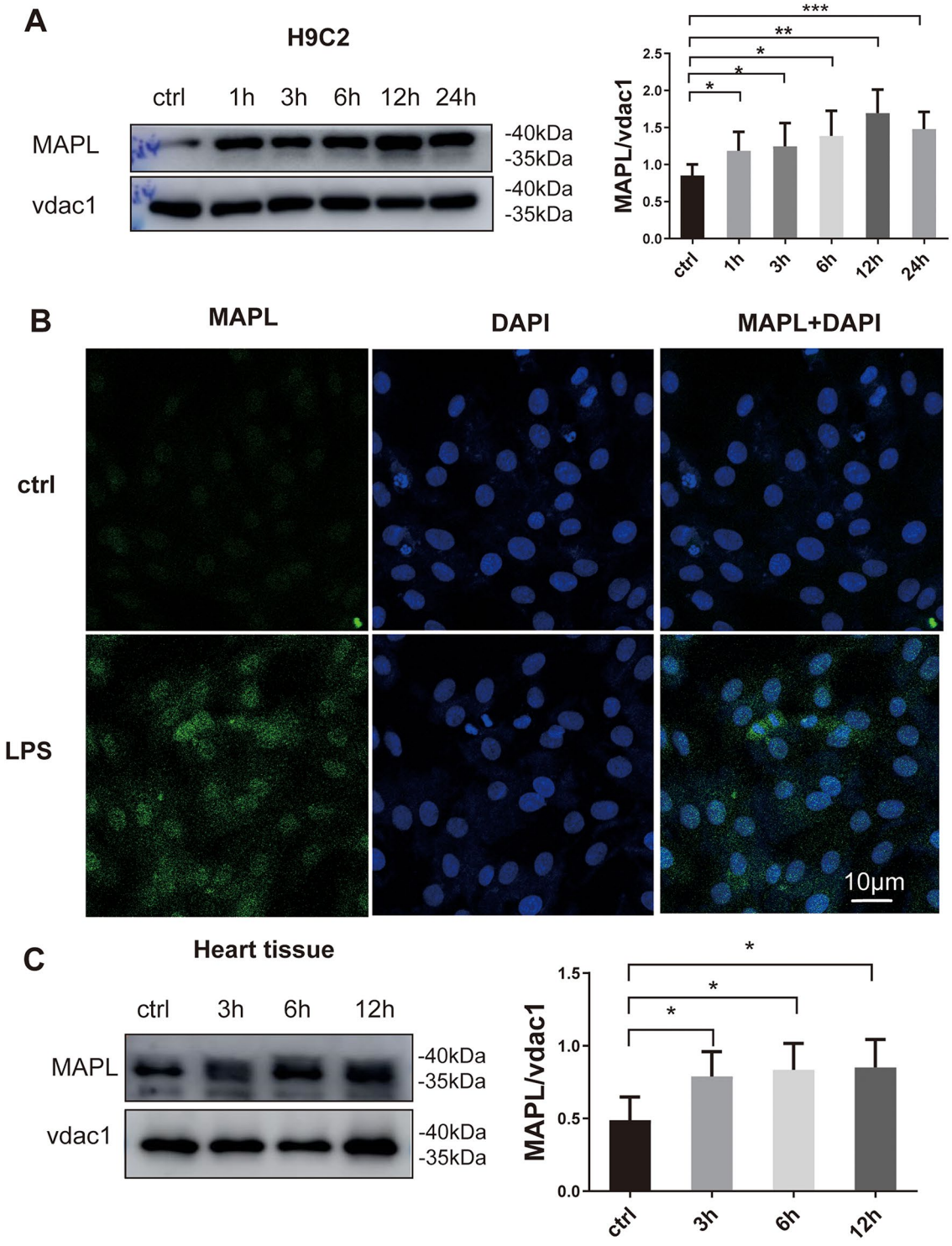

Fig. 1 Expression of MAPL in heart tissue and H9C2 cardiomyocytes were upregulated after LPS stimulation or CLP Challenge. **A**. H9C2 cardiomyocytes were treated with LPS (20 μg/ml) for 1, 3, 6, 12, and 24 h, and the expression of MAPL in mitochondria of cardiomyocytes was analyzed by western blot (*$P < 0.05$, **$P < 0.01$, ***$P < 0.001$, $n = 6$ repeated experiments). **B**. H9C2 cardiomyocytes were treated with LPS for 24 h, then immunofluorescence staining was performed to detect the expression of MAPL (scale bar = 10 μm. $n = 5$ repeated experiments). **C**. Heart tissues were harvested 3, 6, and 12 h after CLP, and the expression of MAPL in mitochondria of heart tissues was analyzed by western blot (*$P < 0.05$, $n = 5$ for each group)

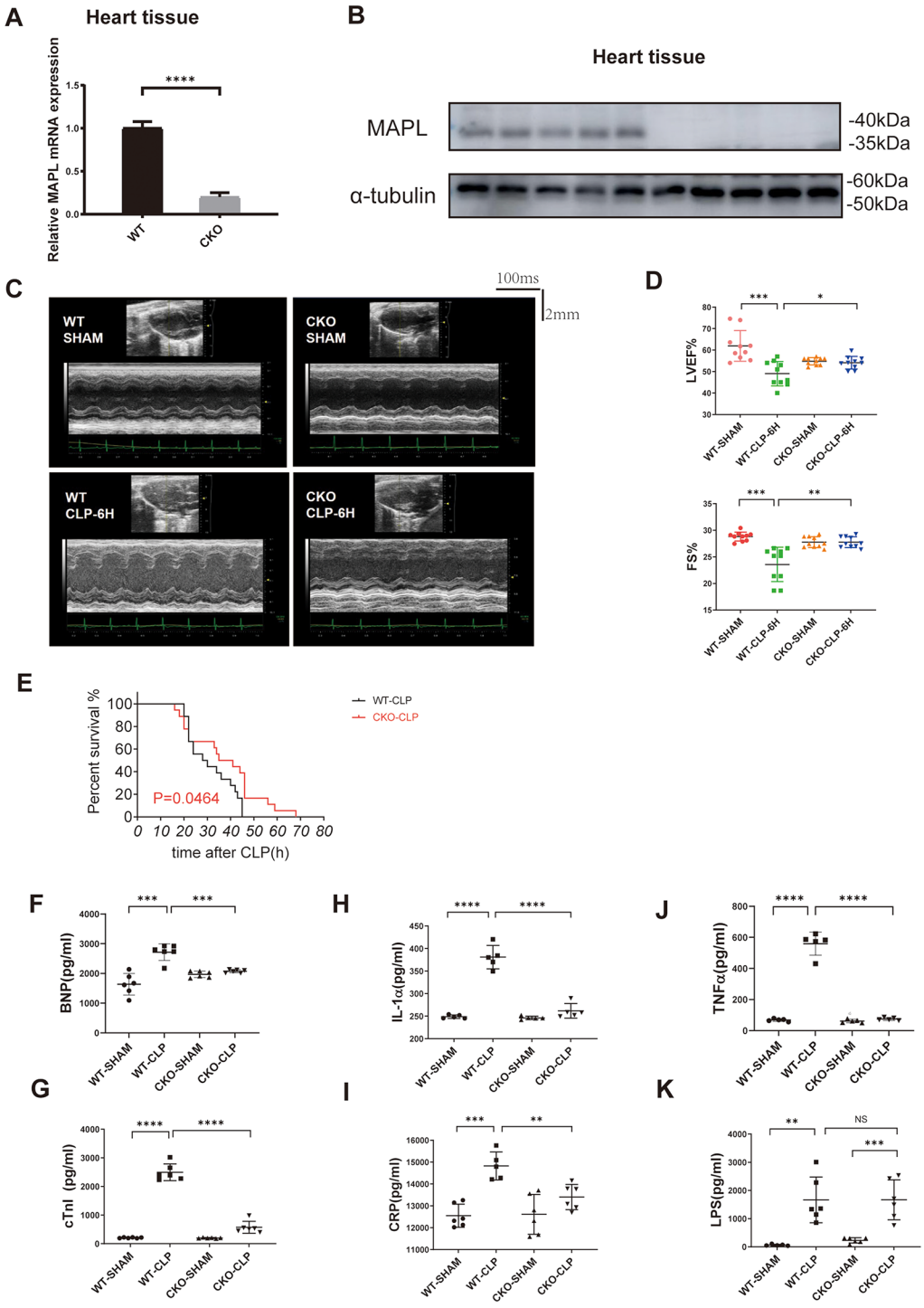

Fig. 2 MAPL deletion improves myocardial dysfunction and attenuates inflammation in CLP-induced sepsis. **A**. The mRNA level of MAPL in heart tissues of WT and MAPL CKO mice (****$P < 0.0001$, $n = 6$ for each group). **B**. The protein level of MAPL in heart tissues of WT and MAPL CKO mice was determined by western blot ($n = 5$ for each group). **C**. Echocardiographic analysis of WT and MAPL CKO mice at 6 h after CLP or sham surgery. **D**. Quantification of echocardiography parameters in **C** (LVEF% and FS%, $n = 10$ for each group, *$P < 0.05$, **$P < 0.01$, ***$P < 0.001$). **E**. The survival data of WT and MAPL CKO mice were recorded 70 h after CLP (WT-CLP, CKO-CLP, $n = 18$ for each group). **F** and **G**. The levels of BNP and cTnI in serum were detected by ELISA (***$P < 0.001$, ****$P < 0.0001$, $n = 6$ for each group). **H**-**J**. The levels of IL-1α, TNFα, and CRP in serum were detected by ELISA (**$P < 0.01$, ***$P < 0.001$, ****$P < 0.0001$, $n = 6$ for each group). **K.** The LPS concentration in serum was detected by ELISA (**$P < 0.01$, ***$P < 0.001$, $n = 6$ for each group)

overexpression (Fig. S7). Additionally, immunofluorescence results indicated that MAPL knockdown suppressed the LPS-induced increase in Bax levels in H9C2 cardiomyocytes (Fig. 3C). Correspondingly, TUNEL assay results showed an increase in the number of TUNEL-positive cells after LPS stimulation, which was reduced following MAPL knockdown (Fig. 3D). Since pathogens typically shift from apoptosis to necroptosis to evade the natural immune response, we then examined the effect of MAPL knockdown on LPS-induced necroptosis. Similarily, the increasing expression of caspase 8 and RIPK3 after LPS stimulation was reversed by MAPL knockdown (Fig. S8).

MAPL deficiency mitigates CLP-induced mitochondrial abnormalities and oxidative stress

Mitochondria in cardiomyocytes are essential for sustaining heart function through the continuous production of ATP, regulation of ROS production, calcium homeostasis, and apoptosis [12]. Given the high mitochondrial density in cardiomyocytes, excessive fission leads to mitochondrial fragmentation, culminating in mitochondrial dysfunction, impaired cellular metabolism, and the initiation of apoptosis [13]. Therefore, in the subsequent study, we investigated the impact of MAPL on mitochondrial structure and function in cardiomyocytes. TEM analysis revealed an increase in mitochondrial number, while the mitochondrial aspect ratio (maximum diameter/minimum diameter) and the number of intact mitochondrial cristae decreased following LPS stimulation. These alterations were ameliorated upon MAPL knockdown (Fig. 4A-D). Comparable results were observed in heart tissues from WT and MAPL-CKO mice (Fig. 4E-H). Additionally, we evaluated ATP production, a key indicator of mitochondrial function. The results indicated that both CLP and LPS stimulation led to reduced ATP production in mouse heart tissues and H9C2 cardiomyocytes. This reduction in ATP production was suppressed in MAPL-CKO mice or MAPL-knockdown H9C2 cardiomyocytes (Fig. 4I-J). We also investigated OCR by SEAHORSE and showed as Fig. S9. Compared with the control group, LPS stimulation decreased basal OCR, ATP production and maximal oxygen consumption, while MAPL knockdown improved basal OCR, ATP production and maximal oxygen consumption after LPS stimulation.

Consistent with previous findings, JC-1 staining results indicated a decrease in mitochondrial membrane potential (MMP) following 24 h of LPS stimulation, which was reversed upon MAPL knockdown (Fig. 4K). Additionally, the DCFH-DA probe results demonstrated that the increase in ROS production induced by LPS stimulation was mitigated by MAPL knockdown (Fig. 4L). An ROS scavenger, NAC significantly reduced LPS-induced production of ROS (Fig. S10). These findings suggest that MAPL deficiency ameliorates LPS- or CLP-induced mitochondrial structural and functional abnormalities.

MAPL promotes drp1-mediated mitochondrial fission in SCM

Considering the role of MAPL in regulating mitochondrial dynamics through targeting drp1 and mfn2 [5], we extracted mitochondria from mouse heart tissues and H9C2 cardiomyocytes to determine the expression levels of drp1 and mfn2. Western blotting results revealed that the protein level of drp1 in the mitochondria of heart tissues increased at 3, 6, and 12 h post-CLP. In contrast, the expression level of mfn2 decreased at 6 and 12 h (Fig. 5A). Similarly, the protein level of drp1 in the mitochondria of H9C2 cardiomyocytes increased over time following LPS stimulation, which was associated with a gradual decrease in mfn2 since 3 h after LPS stimulation (Fig. 5B). These results suggest that mitochondrial dynamics are involved in SCM. Furthermore, the increase in mitochondrial drp1 in CLP-operated mice or LPS-treated H9C2 cardiomyocytes was suppressed by MAPL knockout or knockdown (Fig. 5C-D). Subsequently, the expression of mitochondrial fragments was assessed using immunofluorescent staining. We observed that the number of mitochondrial fragments in H9C2 cardiomyocytes increased following LPS stimulation, which was reduced by MAPL knockdown (Fig. 5E). Collectively, these findings indicate that MAPL deficiency ameliorates mitochondrial dysfunction by preventing drp1-mediated mitochondrial fission.

MAPL promotes SUMOylation of drp1 in SCM

MAPL has been suggested to act as a SUMO E3 ligase for a series of mitochondrial proteins [14]. SUMO1 conjugates mitochondrial dynamics-related proteins to contribute to mitochondrial fission [15]. We subsequently investigated the impact of MAPL on the SUMOylation of total mitochondrial proteins under septic conditions. Mitochondria were isolated from H9C2 cardiomyocytes and mouse heart tissues. Our results indicated an elevated level of total SUMO1-conjugated mitochondrial proteins, but not SUMO2/3 conjugates, in H9C2 cardiomyocytes following LPS treatment. This increase was mitigated by MAPL knockdown (Fig. 6A and Fig. S11). Similarly, the level of mitochondrial SUMO1 conjugates in heart tissues was elevated following CLP, and this effect was suppressed by MAPL knockout (Fig. 6B).

It has been reported that MAPL contributes to mitochondrial fission by catalyzing SUMOylation of drp1 [7], enhancing drp1 protein stability and drp1 association with mitochondria during apoptosis [8]. As previously confirmed, MAPL knockout or knockdown suppressed the CLP- or LPS-induced elevation of drp1. This led us to

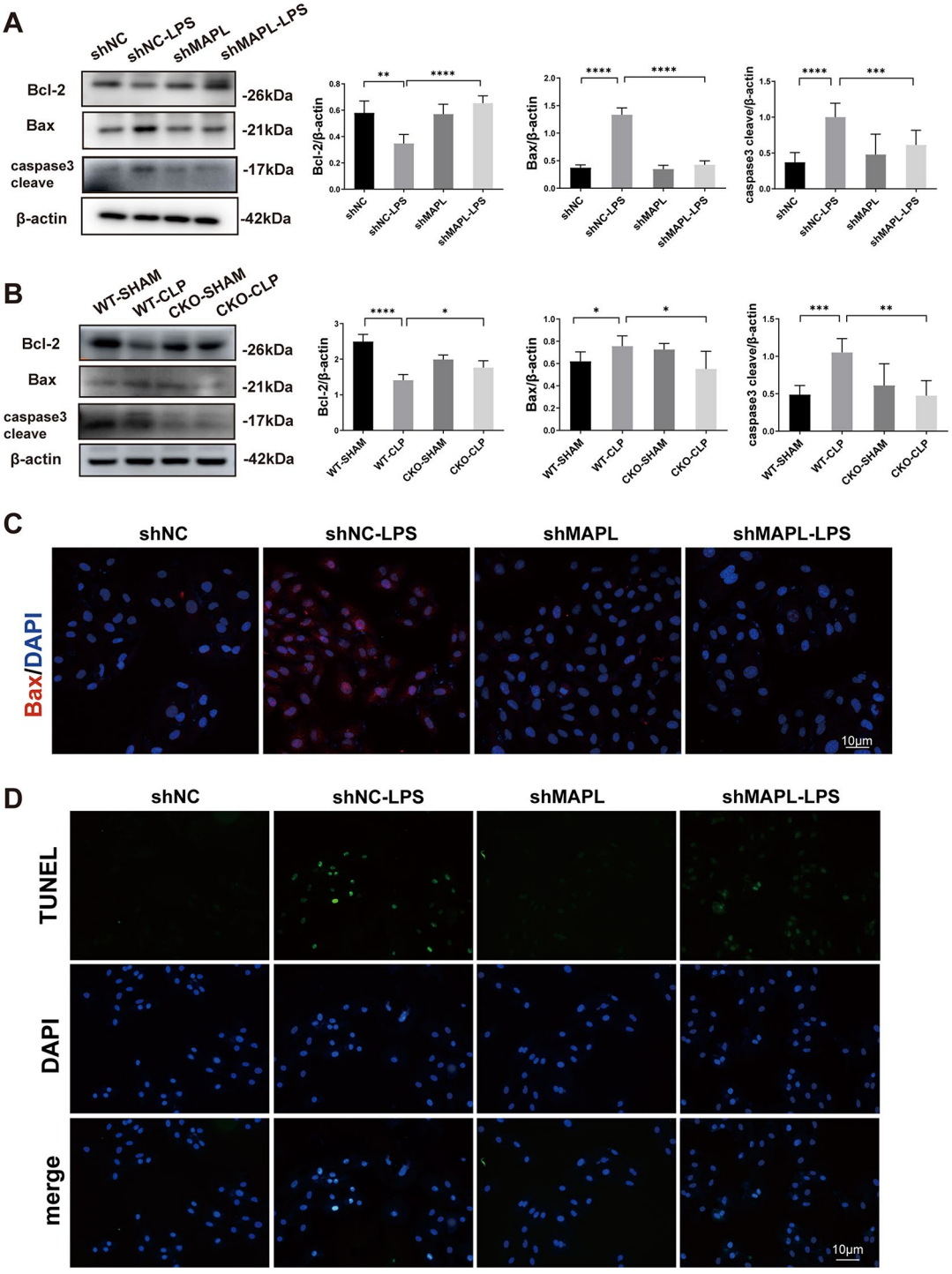

Fig. 3 MAPL deficiency alleviates apoptosis of cardiomyocytes during SCM. **A**. The protein levels of Bcl-2, Bax, and cleaved-caspase 3 in shNC and shMAPL cardiomyocytes after LPS (20 μg/ml) treatment were detected by western blot (**$P < 0.01$, ***$P < 0.001$, ****$P < 0.0001$, $n = 5$ repeated experiments). **B**. The protein levels of Bcl-2, Bax, and cleaved-caspase 3 of heart tissues from WT and CKO mice after sham surgery or CLP were detected by western blot (*$P < 0.05$, **$P < 0.01$, ***$P < 0.001$, ****$P < 0.0001$, $n = 5$ for each group). **C**. Immunofluorescence staining was performed to detect the expression of Bax in shNC and shMAPL cardiomyocytes after LPS (20 μg/ml) treatment (scale bar = 10 μm. $n = 5$ repeated experiments). **D**. TUNEL staining of shNC and shMAPL cardiomyocytes after LPS (20 μg/ml) treatment was detected by TUNEL BrightGreen Apoptosis Detection Kit (scale bar = 10 μm. $n = 5$ repeated experiments)

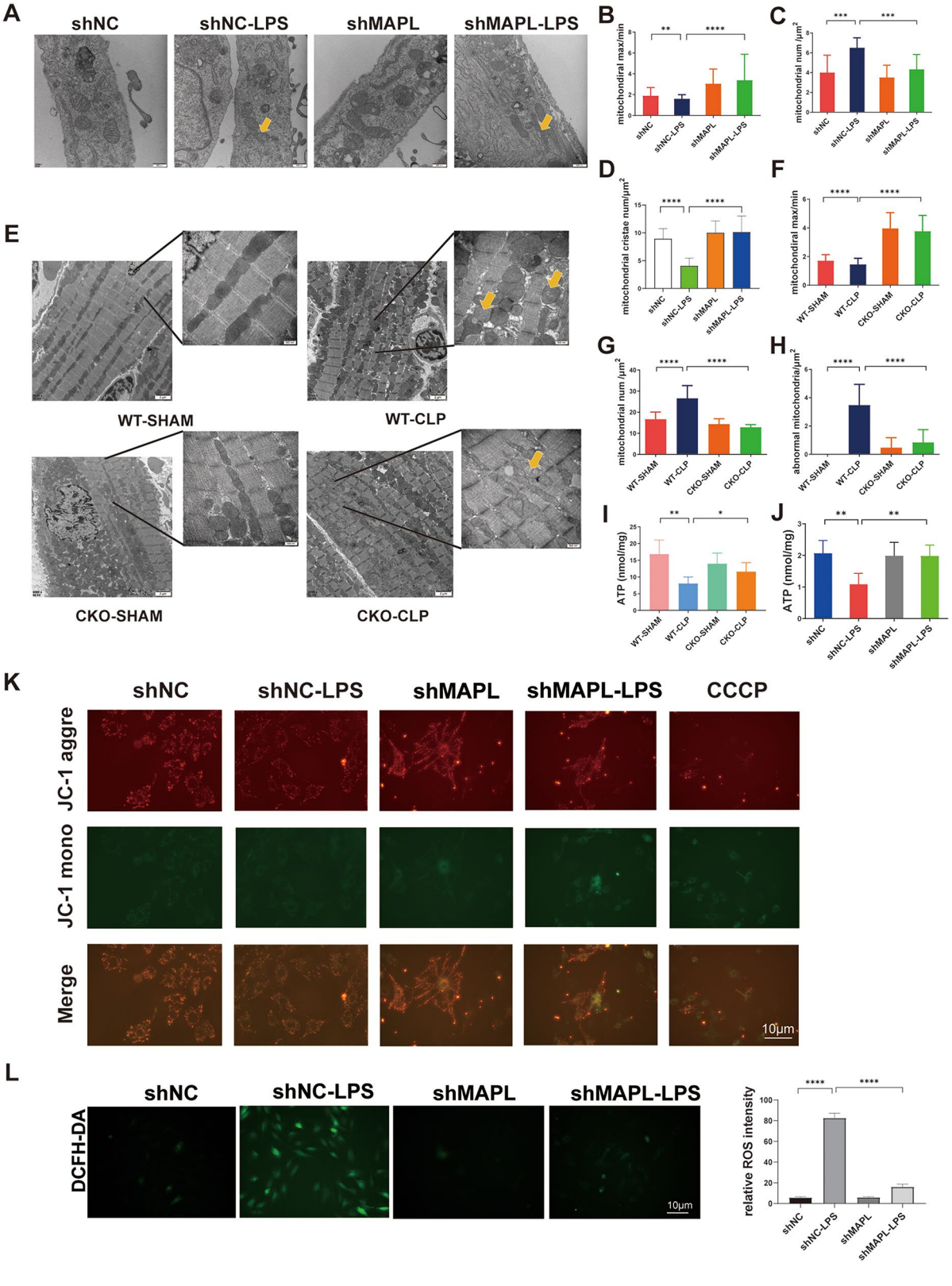

Fig. 4 (See legend on next page.)

(See figure on previous page.)

Fig. 4 MAPL deficiency prevented CLP-induced mitochondrial fission. **A**. Transmission electron microscopy images of H9C2 cardiomyocytes after MAPL knockdown. Yellow arrows indicate abnormal mitochondria in the cardiomyocytes. **B**-**D**. Quantification of mitochondria-related parameters from **A**. **B**. Mitochondrial aspect ratio refers to the ratio of mitochondrial maximum diameter to minimum diameter (**$P < 0.001$, ****$P < 0.0001$, $n = 6$ repeated experiments). **C**. Mitochondrial number/μm^2 refers to the ratio of mitochondrial number to image area (***$P < 0.001$, $n = 6$ repeated experiments). **D.** Mitochondrial cristae numbers/μm^2 refers to the ratio of intact mitochondrial cristae to image area (****$P < 0.0001$, $n = 6$ repeated experiments). **E**. Transmission electron microscopy images of WT and MAPL CKO mice heart tissues after sham or CLP procedures. **F**, **G** and **H.** Quantification of mitochondria-related parameters from E. **F**. Mitochondrial aspect ratio refers to the ratio of mitochondrial maximum diameter to minimum diameter (****$P < 0.0001$, $n = 6$ for each group). **G**. Mitochondrial num/μm^2 refers to the mitochondrial number to the image area (****$P < 0.0001$, $n = 6$ for each group). **H**. Abnormal mitochondrial number refers to abnormal mitochondria to image area (****$P < 0.0001$, $n = 6$ for each group). **I**. ATP concentration in heart tissue of mice was determined after CLP or sham surgery (*$P < 0.05$, **$P < 0.001$, $n = 5$ for each group). **J**. ATP concentration in H9C2 cardiomyocytes was determined after MAPL knockdown (**$P < 0.01$, $n = 5$ repeated experiments). **K**. MMP of shNC-and shMAPL-cardiomyocytes treated with LPS (20 μg/ml) was detected by JC-1 kit (green: monomer, red: aggregates, CCCP was used as a positive control, scale bar = 10 μm, $n = 5$ repeated experiments). **L**. The ROS level in shNC- and shMAPL-cardiomyocytes treated with LPS (20 μg/ml) was detected by DCFH-DA staining. Scale bar = 10 μm (****$P < 0.0001$, $n = 5$ repeated experiments)

investigate whether the SUMOylation of drp1 is dependent on MAPL, thereby resulting in drp1 accumulation. To address this, we conducted co-immunoprecipitation assays to evaluate the SUMOylation status of drp1 under both physiological and septic conditions. Our findings indicated that SUMOylation of drp1 in heart tissues and H9C2 cardiomyocytes was enhanced following CLP or LPS stimulation (Fig. 6C-D). Moreover, we observed a reduction in drp1 SUMOylation following MAPL knockout or knockdown (Fig. 6E-F). These results suggest that MAPL expression is upregulated after sepsis, which facilitates drp1 SUMOylation, thus promoting the protein stability of drp1.

Finally, to investigate the relevance of our findings in human SCM, we measured the protein levels of MAPL and drp1 in heart valve tissues from patients with infective endocarditis (IE) or degenerative valve regurgitation who underwent valve replacement or repair surgery. The result showed that the protein levels of MAPL and drp1 in patients with infective endocarditis were higher than those of patients with degenerative valvular disease (Fig. 6G). These findings suggest the human relevance of MAPL-drp1 pathway in the regulation of SCM.

Discussion

There are numerous potential mechanisms for SCM, including mitochondrial dysfunction, metabolic reprogramming, excessive production of ROS, and disorder of calcium regulation [16–19]. However, the exact pathophysiologic mechanisms leading to cardiac dysfunction still need to be well clarified. To our knowledge, mitochondrial dysfunction plays a pivotal role in SCM. Improving mitochondrial quality control may be beneficial for treating SCM [20]. Our present study provides the first evidence that MAPL expression is increased in cardiomyocytes under sepsis conditions. We further reveal that MAPL mediates drp1-SUMOylation, which results instability and increased drp1 in cardiomyocytes. Moreover, the increased drp1 may facilitate mitochondrial fission and cardiomyocyte apoptosis. Thus, MAPL-mediated drp1-SUMOylation is critical to SCM.

Previous study has reported that MAPL is associated with NF-κB signaling, mitochondrial dynamics, cell death, inflammation, and mitophagy [21]. It is also demonstrated that MAPL is required for mitochondrial fragmentation and cardiac hypertrophy [22], indicating the relationship between MAPL and cardiovascular diseases, especially mitochondrial dysfunction-related disorders. We first investigated the expression pattern of MAPL under sepsis conditions and found that either LPS stimulation or CLP challenge induced increased expression of MAPL in cardiomyocytes (Fig. 1), indicating that MAPL may be associated with the progression of SCM. In addition, we found that LPS at a low dosage (10 mg/kg) did not greatly affect LVEF, while LPS at 20 mg/kg and 30 mg/kg significantly reduced LVEF. The protein level of MAPL increased after LPS injection at a low dosage and rose in a dose-dependent manner (Fig. S2). These results indicated that the protein level of MAPL increased at an early stage of SCM. Surprisingly, the mRNA level of MAPL was increased 3 h after CLP and then decreased gradually, suggesting that the expression of MAPL may be regulated by other factors or affected by post-translational modification during sepsis (Fig. S1). Several sepsis models in animals have been reported for attempting to simulate human sepsis, including injection of pathogen components (e.g. endotoxins), administration of live bacteria (e.g. intravenous, intraperitoneal or intratracheal injection of bacteria), disruption of the host barriers resulting in polymicrobial sepsis (e.g. cecal ligation and puncture, CLP). CLP model is considered the gold standard in sepsis-related research for its close resemblance to the progression and characteristics of sepsis in human [23]. Therefore, CLP was applied in our study.

Then, we performed echocardiography to detect the cardiac function of mice 3, 6, and 12 h after CLP operation. We found that LVEF and CO were significantly reduced at 6 h and 12 h after CLP challenge, but the LVEF was slightly increased at 12 h after CLP (Fig. S4). It could be due to decreased in left ventricle diameter caused by the loss of preload during sepsis [23]. In the next study, we investigated the effect of MAPL on cardiac

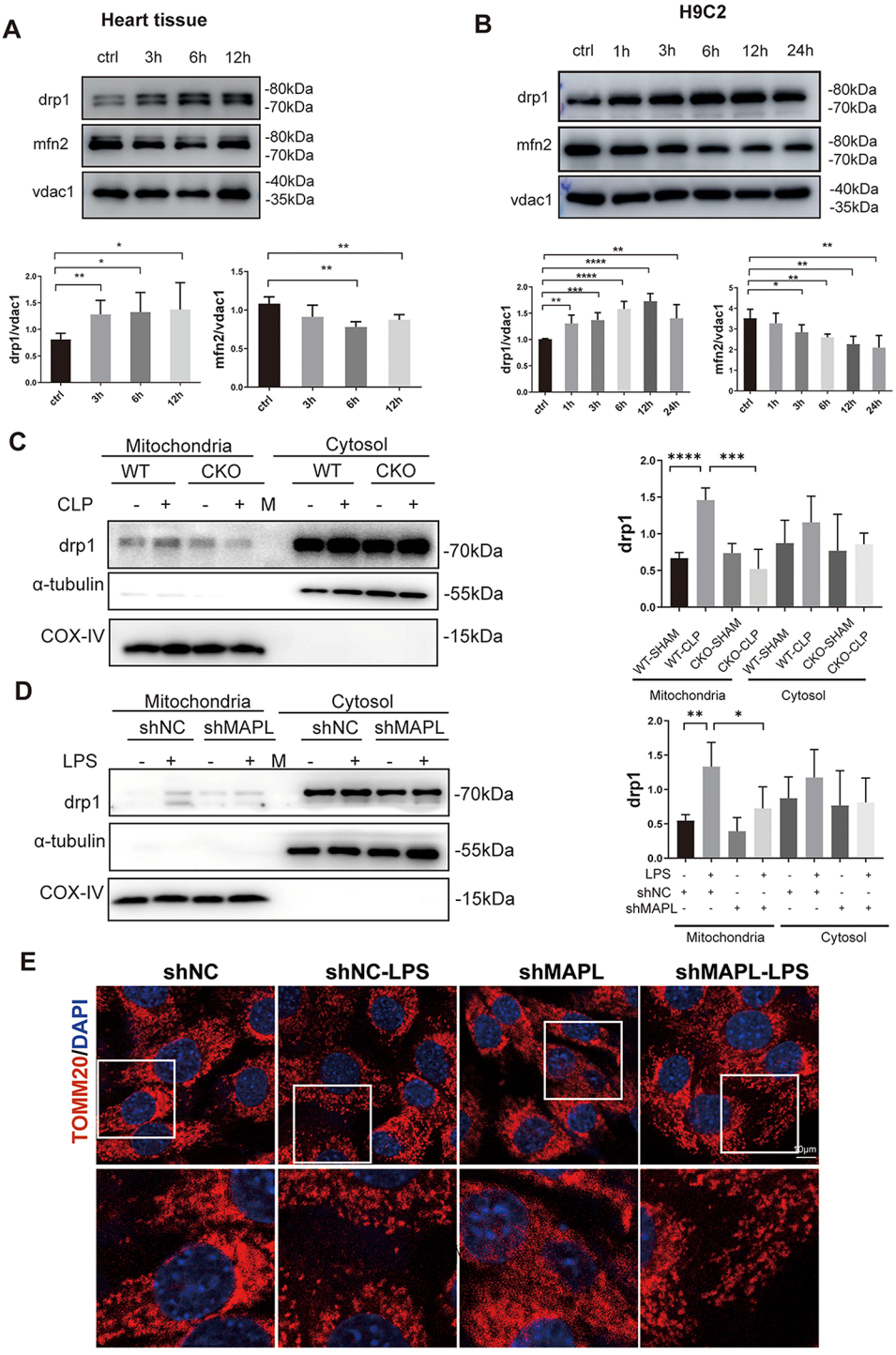

Fig. 5 MAPL knockout or knockdown suppressed CLP or LPS-induced increase of drp1 in heart tissues and H9C2 cardiomyocytes. **A**. The protein levels of drp1 and mfn2 in heart tissue of mice were determined by westernblot (*$P < 0.05$, **$P < 0.01$, $n = 5$ for each group). **B**. The protein levels of drp1 and mfn2 in H9C2 cardiomyocyte were determined by westernblot (*$P < 0.05$, **$P < 0.01$, ***$P < 0.001$, ****$P < 0.0001$, $n = 6$ repeated experiments). **C**. The expression of drp1 in mitochondria of heart tissues from WT or CKO mice after sham surgery or CLP was detected by western blot (***$P < 0.001$, ****$P < 0.0001$, $n = 5$ for each group). **D**. The expression of drp1in mitochondria of shNC- and shMAPL-cardiomyocytes after LPS (20 μg/ml) treatment was detected by western blot (*$P < 0.05$, **$P < 0.01$, $n = 5$ repeated experiments). **E**. Immunofluorescence staining was performed to detect the expression of mitochondrial fragment in shNC- and shMAPL-cardiomyocytes after LPS (20 μg/ml) treatment (scale bar = 10 μm. $n = 5$ repeated experiments)

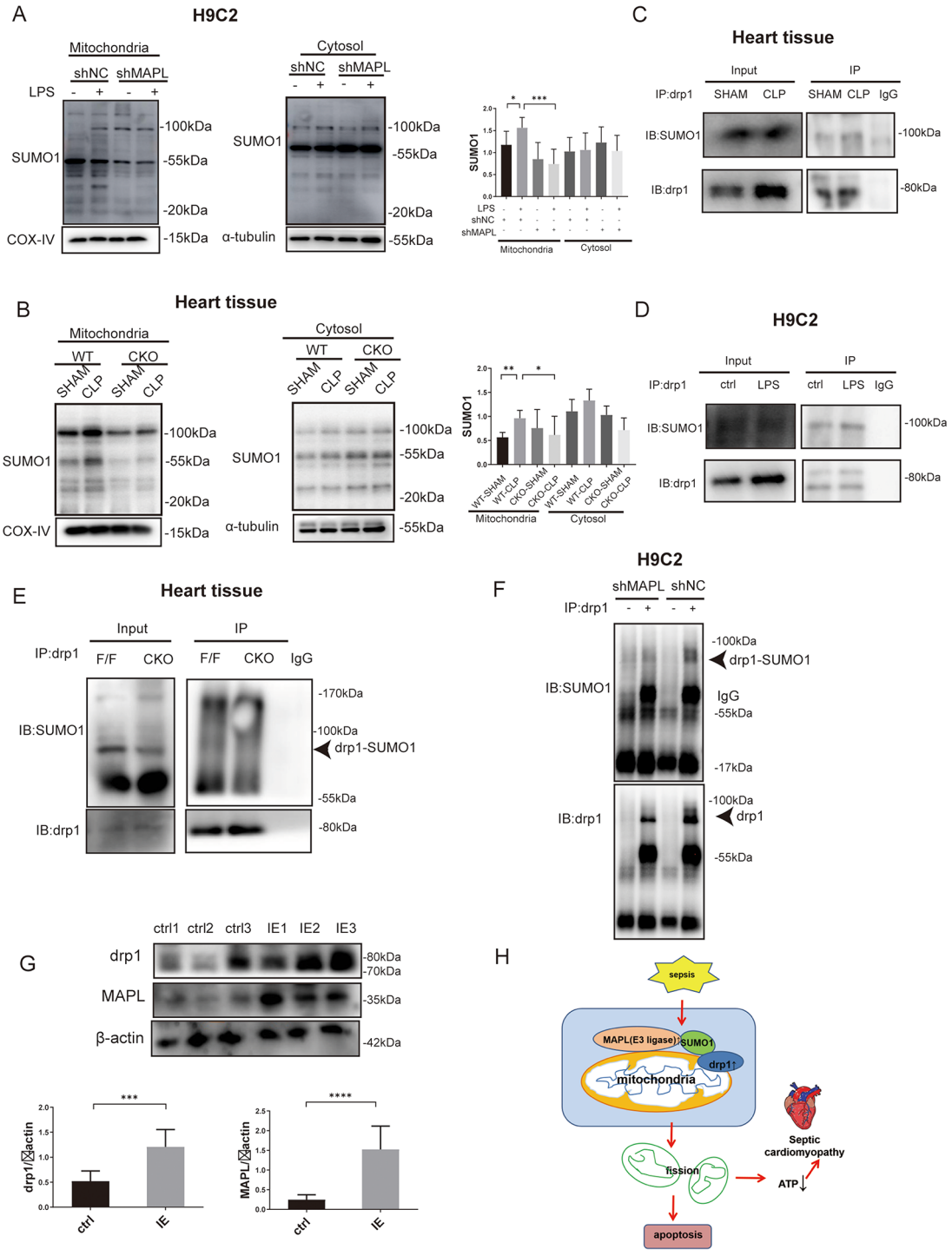

Fig. 6 MAPL promotes SUMOlyation of drp1 in SCM. **A**. The protein levels of SUMO1 in mitochondria of shNC- and shMAPL-cardiomyocytes after LPS (20 μg/ml) treatment were detected by western blot (*$P < 0.05$, ***$P < 0.001$, $n = 5$ repeated experiments). **B**. The protein levels of SUMO1 in mitochondria of heart tissues from mice after sham or CLP challenge were detected (*$P < 0.05$, **$P < 0.01$, $n = 5$ for each group). **C-F**. Whole lysates of heart tissues or H9C2 cardiomyocytes after CLP challenge or LPS treatment were immunoprecipitated and then immunoblotted with antibodies against the indicated proteins. $n = 3$ repeated experiment. **G**. The protein level of MAPL and drp1 in human valve tissues were detected by western blot (***$P < 0.001$, ****$P < 0.0001$, $n = 3$ for each group). **H**. Schematic diagram of this study. Deficiency or knockdown alleviates SCM by reducing drp1-SUMOylation as well as drp1-mediated mitochondrial dysfunction and cardiomyocyte apoptosis

function 6 h after CLP. Our result showed that MAPL-deficiency alleviated CLP-induced decrease of LVEF and FS. Accordingly, the level of BNP reduced and the survival rate improved after MAPL deficiency (Fig. 2E-F). cTnI, a marker of myocardial injury was still increased in MAPL deficient mice after CLP, but it exerted a downward trend compared with WT CLP-operated mice. These results suggest that MAPL deficiency can ameliorate CLP-induced myocardial dysfunction in mice.

Inflammation is a key driver of sepsis since blocking TLR4/NF-κB/NLRP3 pathway improves sepsis-induced myocardial dysfunction [24]. Thus, we determined the effect of MAPL on systemic inflammation. After CLP operation, we found a reduced production of inflammatory cytokines including IL-1α, IL-1β, IL-6, TNFα and CRP in the serum of MAPL deficient mice, implying that MAPL exhibits a pro-inflammatory effect in sepsis (Fig. 2H-J, S5). Apoptosis is a well-defined type of cell death that is involved in SCM. Activation of various caspases, the effectors of apoptosis, and mitochondrial cytochrome c release have been reported in cardiomyocytes following septic challenge [25, 26]. Therefore, anti-apoptotic strategies are beneficial for the improvement of cardiac dysfunction. In our present study, we found that MAPL deficiency mitigates cardiomyocyte apoptosis and necroptosis during SCM (Fig. 3, S7, S8), suggesting that MAPL participates in cell apoptosis and necroptosis during SCM.

Considering MAPL is a mitochondrial outer membrane-anchored protein involved in mitochondrial dynamics, mitophagy, immune response, inflammation and cell apoptosis [5], we tested whether MAPL would influence mitochondrial structure in cardiomyocytes. As expected, we observed that MAPL deficiency alleviated CLP-induced mitochondrial structure damage (Fig. 4A-H). Accordingly, compared with the control group, LPS stimulation decreased basal OCR, ATP production, and maximal oxygen consumption, while MAPL knockdown improved basal OCR, ATP production, and maximal oxygen consumption after LPS stimulation (Fig. 4I-J, S9). It is well known that mitochondrial abnormality will place the cardiomyocytes at risk of ATP depletion. Previous study verified that aberrations of the activity of the respiratory chain and ATP production may be considered a core of mitochondrial dysfunction [27]. Therefore, our results confirm that MAPL deficiency ameliorates SCM by mitigating mitochondrial dysfunction.

It has been well described that alteration in mitochondrial dynamics (fission, fusion, and mitophagy) results in oxidative stress and mitochondrial dysfunction [28]. Previous studies report that excessive mitochondrial fission contributes to cell apoptosis and SCM [29–31]. Mitochondrial fission during apoptosis is mediated by drp1, a target of multiple post-translational modifications, including SUMOylation [32]. As confirmed above, MAPL deficiency alleviated CLP-induced mitochondrial abnormality and reduced mitochondrial number, we wondered that whether MAPL would influence the expression of drp1 in cardiomyocytes during sepsis. Drp1 is transported from the cytoplasm to the mitochondria, where it assembles into helical oligomers that wrap around the mitochondrial outer membrane and promote contraction and breakage in a GTP-dependent manner [33]. Thus, we extracted mitochondria from cardiomyocytes under physiological or pathological conditions and found that the protein level of drp1 in mitochondrial increased after LPS stimulation or CLP challenge, which was inhibited by MAPL knockdown or knockout (Fig. 5). It has been reported that both mfn2 and drp1 are MAPL targets, whose levels also concomitantly change in other pathological conditions, such as ischemic stroke [34]. MAPL reduces mfn2 levels through ubiquitination and stabilizes drp1 through SUMOylation. A Previous study also reported that mfn2 expression was decreased in heart tissues of mice after CLP [35]. Our result consistently showed that the protein level of mfn2 decreased after CLP or LPS stimulation (Fig. 5). However, whether the increased MAPL contributes to mfn2 degradation during SCM needs to be further studied in the future.

Several post-translational modifications including phosphorylation, ubiquitination, sumoylaiton, and nitrosylation regulate mitochondrial fission proteins. MAPL is the first discovered SUMO E3 ligase, which is anchored on the outer membrane of mitochondria with a Ring-finger domain. Thus, we determined the effect of MAPL on SUMOylation of total mitochondrial proteins, and our data confirmed that MAPL promotes SUMOylation of mitochondrial proteins by SUMO1. Previous reports revealed that SUMO1-modified drp1 was preferentially localized to mitochondria, promoting fragmentation and apoptosis, while the SUMO2/3 modification repressed drp1 recruitment to mitochondria, thereby reducing cell death [36–40]. Although it has been demonstrated that MAPL SUMOylates drp1 at the endoplasmic reticulum/mitochondria contact sites during cell death [41], whether MAPL-mediated SUMOylation of drp1 is involved in SCM remains unknown. In the subsequent study, we addressed this question, and found that SUMOylation of drp1 was increased in SCM, and was restrained by MAPL deficiency, indicating that MAPL-induced SUMOylation of drp1 might be essential for the development of SCM (Fig. 6A-F).

In addition, our study still has several limitations. Our present study only investigated MAPL-mediated SUMOylation of drp1 in SCM. There may be other MAPL substrates involved in mitochondrial dysfunction. Additionally, although we found that MAPL deficiency ameliorates SCM, what phenotype would be observed

if MAPL is overexpressed in cardiomyocytes? Will it aggravate SCM? These need to be further investigated in future studies.

The results presented here show that MAPL serves as an incentive for SCM and contributes to promoting cardiomyocyte apoptosis and cardiac dysfunction. Moreover, the MAPL-drp1pathway is essential in favoring mitochondrial fission and apoptosis during SCM. Thus, our findings provide new insights into the pathogenic mechanism of SCM, and targeting MAPL is a potential therapeutic approach for SCM.

Supplementary Information

The online version contains supplementary material available at https://doi.org/10.1186/s12967-024-05836-x.

Supplementary Material 1

Acknowledgements

This work was supported by grants from the National Natural Science Foundation of China (numbers 81830010, 82130012, 82100447), Clinical Research Plan of SHDC (number SHDC2020CR1039B).

Author contributions

Author contributions(I) Conception and design: Ben He; (II) Echocardiography: Huanhuan Huo; (III) Animal and laboratory experiments: Yinghua Wang, Xia Wang, Xiying Huang; (IV) Collection and analysis of data: Zhaohua Cai, Qingqi Ji, Yi Jiang, Fei Zhuang, Yi Li; (V) Data analysis and interpretation: Xia Wang, Yinghua Wang, Linghong Shen; (VI) Manuscript writing: All authors; (VII) Final verification and approval of all data and manuscript: All authors.

Data availability

The data that support the findings of this study are available from the corresponding author upon reasonable request.

Declarations

Consent for publication

All authors concur with the submission and publication of this paper.

Conflict of interest

The authors have no relevant financial or non-financial interests to disclose.

Received: 20 June 2024 / Accepted: 31 October 2024
Published online: 11 November 2024

References

1. Hollenberg SM, Singer M. Pathophysiology of sepsis-induced cardiomyopathy. Nat Reviews Cardiol. 2021;18(6):424–34.
2. Lukas Martin M. THE SEPTIC HEART current understanding of Molecular mechanisms and clinical implications. Chest. 2019;2(155):427–37.
3. Wang Y, Z.X.Z.M. Risk factors for postoperative sepsis-induced cardiomyopathy in patients undergoing general thoracic surgery: a single center experience. J Thorac Dis. 2021;13(4):2486–94.
4. Zou R, et al. DNA-PKcs promotes sepsis-induced multiple organ failure by triggering mitochondrial dysfunction. J Adv Res. 2022;41:39–48.
5. Calle X, et al. Mitochondrial E3 ubiquitin ligase 1 (MUL1) as a novel therapeutic target for diseases associated with mitochondrial dysfunction. IUBMB Life. 2022;74(9):850–65.
6. Zhao Y, et al. MiR-485-5p modulates mitochondrial fission through targeting mitochondrial anchored protein ligase in cardiac hypertrophy. Biochim et Biophys Acta (BBA) - Mol Basis Disease. 2017;1863(11):2871–81.
7. Braschi E, Zunino R, McBride HM. MAPL is a new mitochondrial SUMO E3 ligase that regulates mitochondrial fission. EMBO Rep. 2009;10(7):748–54.
8. Wasiak S, Zunino R, McBride HM. Bax/Bak promote sumoylation of DRP1 and its stable association with mitochondria during apoptotic cell death. J Cell Biol. 2007;177(3):439–50.
9. Puri R, et al. Mul1 restrains parkin-mediated mitophagy in mature neurons by maintaining ER-mitochondrial contacts. Nat Commun. 2019;10(1):3645.
10. Yun J, et al. MUL1 acts in parallel to the PINK1/parkin pathway in regulating mitofusin and compensates for loss of PINK1/parkin. eLife. 2014;3:e01958.
11. Xia Wang Yinhua Wang Huanhuan Huo Xin Shi Anwen Yin Qingqing Xiao, He B. Transient receptor vanilloid subtype 4 (TRPV4)-mediated Ca2 + influx promotes glomerular endothelial inflammation in sepsis-associated acute kidney injury. Lab Invest. 2023;6(103):100126.
12. Marín-García J, Akhmedov AT. Mitochondrial dynamics and cell death in heart failure. Heart Fail Rev. 2016;21(2):123–36.
13. Ahmed ME, et al. Synergy in disruption of mitochondrial dynamics by Aβ (1–42) and glia maturation factor (GMF) in SH-SY5Y cells is mediated through alterations in Fission and Fusion proteins. Mol Neurobiol. 2019;56(10):6964–75.
14. Lokireddy S, et al. The Ubiquitin Ligase Mul1 induces mitophagy in skeletal muscle in response to muscle-wasting Stimuli. Cell Metabol. 2012;16(5):613–24.
15. Harder Z, Zunino R, McBride H. Sumo1 conjugates mitochondrial substrates and participates in mitochondrial fission. Curr Biol. 2004;14(4):340–5.
16. Yang H, Zhang Z. Sepsis-induced myocardial dysfunction: the role of mitochondrial dysfunction. Inflamm Res. 2021;70(4):379–87.
17. Lin Y, Xu Y, Zhang Z. Sepsis-Induced Myocardial Dysfunction (SIMD): the pathophysiological mechanisms and therapeutic strategies targeting Mitochondria. Inflammation. 2020;43(4):1184–200.
18. Kakihana Y et al. Sepsis-induced myocardial dysfunction: pathophysiology and management. J Intensive Care, 2016;4(1):22.eCollection 2016.
19. Martin L, et al. The Septic Heart Current understanding of Molecular mechanisms and clinical implications. Chest. 2019;155(2):427–37.
20. Zhou H, et al. TMBIM6 prevents VDAC1 multimerization and improves mitochondrial quality control to reduce sepsis-related myocardial injury. Metabolism. 2023;140:155383.
21. Puri R, et al. Defending stressed mitochondria: uncovering the role of MUL1 in suppressing neuronal mitophagy. Autophagy. 2020;16(1):176–8.
22. Vásquez-Trincado C, et al. Myristate induces mitochondrial fragmentation and cardiomyocyte hypertrophy through mitochondrial E3 ubiquitin ligase MUL1. Front Cell Dev Biology. 2023;11:107231.
23. Rittirsch D, et al. Immunodesign of experimental sepsis by cecal ligation and puncture. Nat Protoc. 2009;4(1):31–6.
24. Luo M, et al. Ginsenoside Rg1 attenuates cardiomyocyte apoptosis and inflammation via the TLR4/NF-kB/NLRP3 pathway. J Cell Biochem. 2020;121(4):2994–3004.
25. Fauvel H, et al. Differential effects of caspase inhibitors on endotoxin-induced myocardial dysfunction and heart apoptosis. Am J Physiol Heart Circ Physiol. 2001;280(4):H1608–14.
26. NEVIERE R, et al. Caspase inhibition prevents cardiac dysfunction and heart apoptosis in a rat model of sepsis. Am J Respir Crit Care Med. 2001;163(1):218–25.
27. Chistiakov DA, et al. The role of mitochondrial dysfunction in cardiovascular disease: a brief review. Taylor Francis. 2018;England:121–7.
28. Kornfeld OS, et al. Mitochondrial reactive oxygen species at the heart of the Matter. Circul Res. 2015;116(11):1783–99.
29. Mukherjee R, et al. Drp1/p53 interaction mediates p53 mitochondrial localization and dysfunction in septic cardiomyopathy. J Mol Cell Cardiol. 2023;177:28–37.
30. Giacomo Stanzani MRDM. The role of mitochondria in sepsis-induced cardiomyopathy. Biochim Biophys Acta Mol Basis Dis. 2019;4(1865):759–73.
31. Yi L, et al. Cadmium-induced apoptosis of Leydig cells is mediated by excessive mitochondrial fission and inhibition of mitophagy. Cell Death Dis. 2022;13(11):928.
32. Seiya Yamada ASNI. Drp1 SUMO/deSUMOylation by Senp5 isoforms influences ER tubulation and mitochondrial dynamics to regulate brain development. iScience. 2021;12(24):103484.
33. Quiles JM, Gustafsson ÅB. The role of mitochondrial fission in cardiovascular health and disease. Nat Reviews Cardiol. 2022;19(11):723–36.
34. Ren K, et al. Mitochondrial E3 ubiquitin ligase 1 promotes brain injury by disturbing mitochondrial dynamics in a rat model of ischemic stroke. Eur J Pharmacol. 2019;861:172617.

35. Rahim I, et al. Melatonin alleviates sepsis-induced heart injury through activating the Nrf2 pathway and inhibiting the NLRP3 inflammasome. Naunyn Schmiedebergs Arch Pharmacol. 2021;394(2):261–77.
36. Vu LD, Gevaert K, De Smet I. Protein Language: post-translational modifications talking to each other. Trends Plant Sci. 2018;23(12):1068–80.
37. Mendler L, Braun T, Müller S. The Ubiquitin-Like SUMO system and heart function. Circul Res. 2016;118(1):132–44.
38. Henley JM, Carmichael RE, Wilkinson KA. Extranuclear SUMOylation Neurons Trends Neurosciences. 2018;41(4):198–210.
39. Han Z, et al. The post-translational modification, SUMOylation, and cancer (review). Int J Oncol. 2018;52(4):1081–94.
40. Le N-T. Sub-cellular localization specific SUMOylation in the heart. Biochim Biophys Acta Mol Basis Dis. 2017;8(1863):2041–55.
41. Prudent J, et al. MAPL SUMOylation of Drp1 stabilizes an ER/Mitochondrial platform required for cell death. Mol Cell. 2015;59(6):941–55.

Publisher's note